Building hierarchical interfaces using $BaSrTiO_3$ nanocuboid dotted graphene sheets in an optimized percolative nanocomposite with outstanding dielectric properties

Hang Luo,† Kechao Zhou,† Christopher Bowen,‡ Fuqiang Zhang,† Anqi Wei,† Zhong Wu,† Chao Chen,† Dou Zhang*,†

† State Key Laboratory of Powder Metallurgy, Central South University, Changsha, Hunan 410083, China

‡ Department of Mechanical Engineering, University of Bath, Bath, BA2 7AY, UK

Corresponding Authors

*E-mail: dzhang@csu.edu.cn (D. Zhang).

Abstract: High-performance dielectric materials with high permittivity and suppressed dielectric loss are of interest for potential electrical applications. Ceramic/polymer composites show improved permittivity and low dielectric loss but the permittivity is usually limited to less than 100. The permittivity of conductive particles/polymer percolative composites can be dramatically improved by a small loading of conductive fillers, however, which is at the expense of a greatly increased dielectric loss. A dielectric composite that lies between the two kinds of composites that combine increased permittivity from a percolative composite with a suppressed dielectric loss from insulative composites is of interest. In this paper, we report an optimized percolative composite with hierarchical interfaces by dopamine modifying $BaSrTiO_3$ (BST) nanocuboid dotted functionalized graphene sheets (FGS). Due to the hierarchical interfaces, the prevention of contact between FGS by BST nanocuboids and a tight adhesion of Dop@BST@FGS with the polymer matrix, the Dop@BST@FGS/P(VDF-HFP) nanocomposites exhibit a high permittivity of 170.4 and a suppressed dielectric loss of 0.114 at 1kHz. It is notable that the novel composite overcomes the problem of simultaneously realizing high permittivity and low dielectric loss in percolative nanocomposites. The findings of this research can provide a feasible approach to produce high-performance dielectric nanocomposite materials.

Key words: functionalized graphene sheets; percolative nanocomposite; hierarchical interfaces; high permittivity; suppressed dielectric loss

High-performance dielectric materials with high relative permittivity and surpressed dielectric loss are of interest for potential electrical and electronic applications, such as energy storage devices, capacitor, artificial muscles, etc.[1-7] Recently, ceramic/polymer insulative composites that combine high permittivity ferroelectric ceramics ($BaTiO_3$, $Pb(Zr,Ti)O_3$, $Pb(Mg_{1/3}Nb_{2/3})O_3$–$PbTiO_3$, $BaSrTiO_3$ (BST)) with flexible polymers have been examined to exploit the beneficial dielectric properties, insulating properties and flexibility of each phase.[8, 9] However, due to the low permittivity of the polymer matrix phase the maximum relative permittivity that can be achieved is usually limited to less than 100, even when the composite incorporates high levels of ferroelectric ceramic particles (>50% vol). The need for high ceramic loading levels in such composite systems leads to reduced mechanical flexibility and uniformity of the materials.

Conductive particle/polymer (percolative composite) systems have also been regarded as an effective strategy for preparing high-performance dielectric materials. One danger of using conductive additives is that while the permittivity increaes, the dielectric loss can also dramatically increase due to the inevitable agglomeration and connection of the conductive fillers in the percolative composite.[10-12] As a result, it is of interest to the develop new dielectric composites that lie between the two kinds of aforementioned composite that combine increased permittivity from a percolative composite (e.g. graphene/polymer) with a suppressed dielectric loss from insulative composites (e.g. ceramic/polymer).

Graphene with its excellent mechanical, electronic properties, thermal

conductivity, and large specific surface area (2630 $m^2 g^{-1}$) is regarded as an ideal filler in dielectric composites and has been recently investigated.[13-15] Previous reports have indicated that the permittivity of the graphene/polymer composite can be dramatically improved with a small loading of graphene.[16, 17] The existence of uniformly dispersed graphene in the polymer matrix is crucial to achieve a large interface area, which can contribute to the improved permittivity via the Maxwell-Wagner-Sillars interface polarization in the percolative composites.[18-20] Thus, recent efforts have been devoted to improving the dispersibility of graphene in the polymer matrix, and have focused mostly on chemical modification methods.[17, 21] The role of the modifier is to react with the distributed groups of –OH, –COOH, or =O on the surface of the graphene. In practice it is difficult to form a complete coating due to the large specific surface area of graphene. The organic modifier on the graphene surface can also destroy the unique conjugated structure of graphene, which does not contribute to an increase permittivity due to the low permittivity of the modifier itself. Table 1 summarizes the previously reported dielectric properties of percolative nanocomposite with a variety of conductive fillers. As presented in Table 1, the permittivity increases after introducing different amounts of modified conductive fillers, while most of the composites with a high permittivity (>100) exhibit a high dielectric loss.

Table 1. Comparison of dielectric properties at 1 kHz for dielectric nanocomposites with a variety of conductive fillers

Matrix	Filler	Relative permittivity	Dielectric loss	Fraction	Ref.(year)
P(2-IBO)	RGO	8.35	0.11	1.5 wt%	[17] (2015)
PVDF	GND/RGO	~58	~0.041	1.4 wt%	[22] (2015)
Epoxy	GNPs/AFs	11	0.15	2/10 vol%	[23] (2015)
PVDF	MWCNT/C	5910	~2.5	10.4 vol%	[24] (2015)
Epoxy	GNPs/SiC	~12		7.0 wt%	[25] (2014)
PVDF	Ag	~25	~0.7	0.04 wt%	[26] (2013)
Epoxy	graphite	~230	~100	2.73 vol%	[27] (2013)
PMMA	RGO	40.6	0.12	6 wt%	[28] (2012)
PVDF	graphene	~70	~0.8	2.2 vol%	[5] (2012)
PVDF	SiC	~260	1.46	20 vol%	[29] (2011)
PVDF	graphene	662	~3.8	2.4 vol%	[20] (2011)
P(VDF-HFP)	Dop/BST/FGS	170.4	0.114	4.67wt%	This work

RGO: Reduced Graphene Oxide; GND: Graphene nanodot; GNPs: Graphene nanosheets; AFs: Al_2O_3 nanofibers; P(2-IBO): Poly(2-isopropenylbenzoxazole)

In order to enhance the properties of such composites, a novel dielectric nanocomposite based on hierarchical interfaces was investigated. BST ceramic in a nanocuboid form was initially formed as dots to decorate functionalized graphene sheets (FGS). The BST modified FGS was further modified by dopamine (Dop@BST@FGS) before being introduced into the ferroelectric polymer matrix poly(vinylidene fluoride-co-hexafluoropropylene) (P(VDF-HFP)); this acted to improve the interfacial adhesion between the BST@FGS composite particles and the P(VDF-HFP) matrix. The BST nanocuboid decorated functionalized graphene

nanosheets were created by a facile sol-gel method. Due to increased interface area from hierarchical interfaces between the BST, FGS, dopamine, and P(VDF-HFP) and the high permittivity of the BST ferroelectric ceramic, Dop@BST@FGS/P(VDF-HFP) nanocomposites with a high relative permittivity of 170.4 was obtained at 1 kHz. In addition, due to the improved interfacial adhesion and homogeneous dispersion of Dop@BST@FGS, the optimized percolative nanocomposites simultaneously maintained a suppressed dielectric loss of less than 0.114 at 1 kHz. The formation and characterization of nanocomposites with FGS and BST modified FGS clearly indicated that Dop@BST@FGS/P(VDF-HFP) nanocomposites showed the best dielectric properties. It was notable that the creation of hierarchical interfaces in the Dop@BST@FGS composite overcame the problem of simultaneously realizing high permittivity and low dielectric loss in the percolative nanocomposites. Thus, the findings of this research indicate a feasible approach to producing high-performance dielectric nanocomposite.

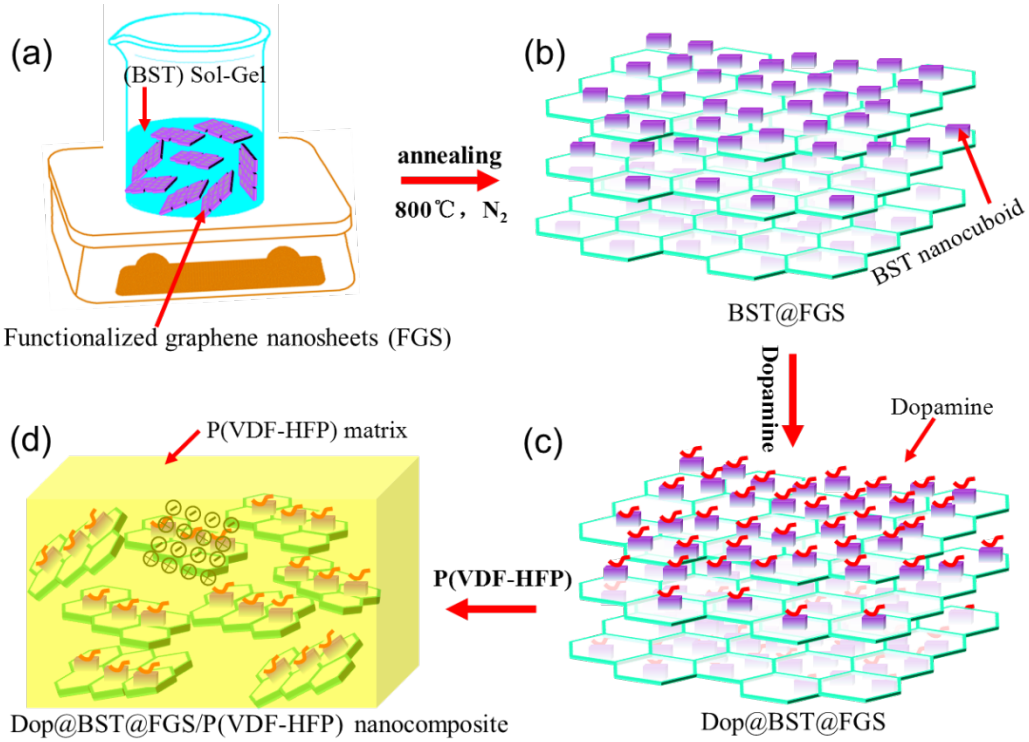

Figure 1. Schematic illustration of preparation route of Dop@BST@FGS/P(VDF-HFP) nanocomposite, (a) functionalized graphene nanosheets, (b) BST nanocuboid dotted FGS composite, (c) Dop@BST@FGS composite particle, and (d) the presence of space charge at the interface in Dop@BST@FGS/P(VDF-HFP) nanocomposite.

RESULTS AND DISCUSSION

Figure 1 illustrates the formation process of the Dop@BST@FGS/P(VDF-HFP) nanocomposite, the precise details proccess of preparing the nanocomposites is shown in the Supporting Information. A series of BTS@FGS composite particles with different mass ratios of BTS:FGS (1:2, 1:1, 2:1) were initially sythesized, the mass ratio of 2:1 was selected due to the formation of BST nanocuboids on FGS, and the FGS content characterized via thermogravitric analysis (TGA) (Supporting Information Figure S1) was approximately 28.7 wt%. The synthesized graphene

nanosheet was thermally exfoliated (Figure 1a) by a simple thermal treatment, and sol-gel method was used to form the BST@FGS composite particle, the FGS was mixed with the BST sol-gel and annealed in N_2 (Figure 1b) to form BST nanodots on the FGS. The existence of the chemical covalent bonding between BST and FGS was proven by X-ray photoelectron spectroscopy (XPS) (Supporting Information Figure S2). The BST@FGS composite particles were then modified by dopamine, as in Figure 1c.

The Dop@BST@FGS was dispersed in P(VDF-HFP) matrix shown in Figure 1d, which also illustrates the accumulation of interfacial charges at the interfaces in the Dop@BST@FGS/P(VDF-HFP) nanocomposite. As reported, the calculated work function for graphene is 4.42 eV,[30, 31] and the Fermi energy level of BST is approximately 4.0 eV;[32, 33] as a result of eletronic transfer from graphene to BST, positive space charges exist at the FGS and negative space charges accumulate at the BST surface (see Figure 1d). A negatively charged layer in the P(VDF-HFP) matrix at its interface between the fillers and the P(VDF-HFP) can form due to the high electronegativity of the fluorine ions (F^-) in P(VDF-HFP) and positive space charges would exist in the dopamine layer due to the polar interaction between the BST@FGS and the P(VDF-HFP) matrix. The high density of space charges which accumulate at the different interfaces in the nanocomposite induce a strong interfacial polarization, which can contribute to the high overall permittivity.

Figure 2a shows the X-ray diffraction (XRD) patterns of the BST@FGS, pristine FGS and BST. It is clear that a small hump at approximately 26^{o} was observed in the XRD pattern of pristine FGS, which was attributed to the (002) reflection of graphite.[34] The small hump implies that the graphene sheets are highly disordered and there is stacking with low degree of graphitization.[35] The same peak is also observed in the XRD patterns of the BST@FGS. The pristine BST shows diffraction peaks at 2θ of 22^{o}, 31^{o}, 39^{o}, 45^{o}, 51^{o}, and 56^{o}, which correspond to the (100), (110), (111), (200), (210) and (211) characteristic peaks of BST and match well with the perovskite peaks based on the powder diffraction file database (#80–1351). It can be seen that all of the diffraction peaks at similar locations of BST and FGS were observed in the XRD patterns of BST@FGS. The XRD of graphite, graphene oxide and reduced graphene oxide indicated pure graphene was synthesized (Supporting Information Figure S3). The results of XRD and Raman spectra (Supporting Information Figure S4) indicate that the BST@FGS was successfully synthesized without any impurity phase.

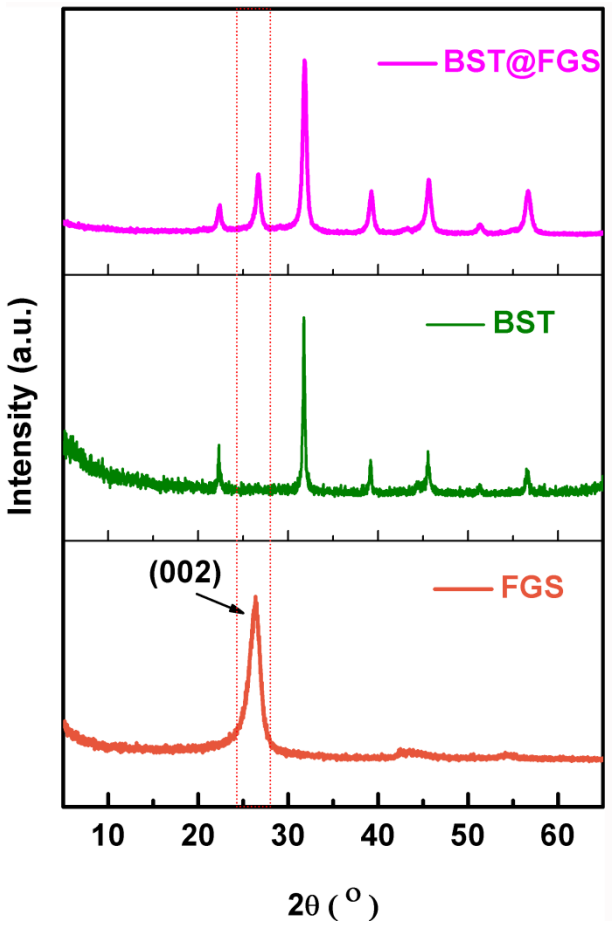

Figure 2. XRD pattern of BST@FGS, BST and FGS

The morphology and microstructure of the FGS, BST@FGS and Dop@BST@FGS were investigated by scanning electron microscopy (SEM) and transmission electron microscopy (TEM), which are shown in Figure 3. Figure 3(a)-3(c) show the morphology of the FGS with numerous wrinkles and folds as a result of the large-surface area and thin graphene nanosheets. The selected area electron diffraction (SAED) pattern (insert in Figure 3c) indicates that the FGS was ultra thin, possibly consisting of one-layer or two-layer graphene;[20, 36] this agrees with observations via atomic force microscope (AFM) (see Supporting Information Figure S5). Figure 3d shows the SEM image of the BST@FGS, the white particles in the view were shown to be BST by energy dispersive spectrometer (EDS) (insert image),

and transmission electron microscope mapping (Supporting Information Figure S6), the elemental ratio is close to the setting chemical composition of $Ba_{0.8}Sr_{0.2}TiO_3$. TEM images of the Dop@BST@FGS with low and high magnifications are presented in Figure 3e and 3f, respectively. It can be seen that BST ceramic with a nanocuboid morphology that is homogeneously decorated on the surfaces of FGS, along with the formation of a polydopamine resin layer coated on the surfaces of each BST nanocuboid; The results of FT-IR further proved that the BST was successfully modified by dopamine (see Supporting Information Figure S7) The morphology of BST can be more clearly observed via the HAADF-STTEM images shown in Figure 3g and 3h. The BST nanocuboids dotted on the surfaces of the FGS prevented the graphene nanosheets from agglomerating together and provided a high surface area. High-resolution transmission electron microscopy (HRTEM) images of BST@FGS composite particles are shown in Figure 3i, the darker region exhibited the clear lattice fringes with interplanar space of 0.248 and 0.398 nm, which can be attributed to the (110) and (100) plane of BST ceramic, and the results were corresponded to the ASED pattern inserted in Figure 3i.

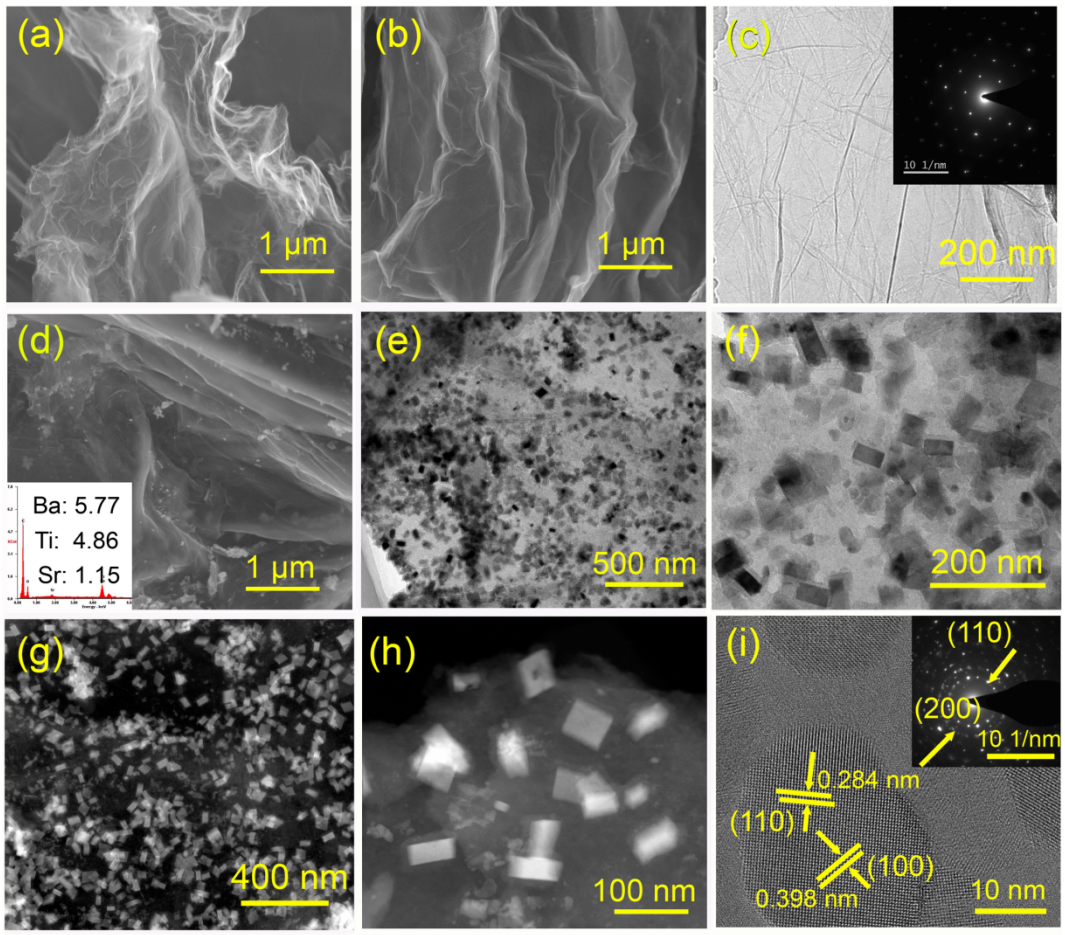

Figure 3. (a)(b) SEM images and (c) TEM image of graphene nanosheets, the inset in (c) shows the SAED pattern of the graphene nanosheets. (d) SEM of the Dop@BST@FGS composite particles with the EDS pattern inset. (e) (f) TEM images of Dop-BST-FGS composite particles at low and high magnifications, respectively. (g) (h) HAADF-STTEM images of the Dop@BST@FGS composite particles. (i) HRTEM image of the Dop@BST@FGS composite particles, and the inset in (i) shows the SAED pattern.

The dielectric properties of the Dop@BST@FGS/P(VDF-HFP) nanocomposites films were investigated as a function of frequency at room temperature. The permittivity, dielectric loss and ac conductivity of the nanocomposite with various

Dop@BST@FGS loadings are shown in Figure 4a-4c. It can be seen that the permittivity of the Dop@BST@FGS/P(VDF-HFP) nanocomposites was similar to the traditional percolative composites,[10] which increased with the increase of the filler loading. The relative permittivity of the composite with 7.19 vol% FGS at 1 kHz attained a value of 170.4 and was increased by 24 times compared to the pure P(VDF-HFP). It was interesting to note that the nanocomposite films showed a relatively stable permittivity up to 1MHz, this is in contrast to the typical response of percolative composites whose permittivity is highly frequency dependent and decreases significantly with increasing frequency.[10, 11, 37] The thickness of the BST nanocuboids in this study is nearly one to two orders of magnitude larger than those of organics based modification layer in most previous reports.[8, 10] As a result, more charge carriers can migrate and accumulate at the interfaces between the BST nanocuboid and the FGS due to the long-distance channel path, which leads to large polarization and high permittivity, and the increased polarization can partly offset the decreased polarization due to the increased frequency.[29] As a result, the nanocomposites showed a relatively stable permittivity with the frequency range. It is thought that the samples exhibited an increased permittivity due to the following reasons: (i) the BST nanocuboid is homogeneously dispersed on the FGS surface, which prevents agglomeration and helps to isolate the graphene nanosheets and also maximizes the specific surface area of the graphene. (ii) the multiple modifications of BST and dopamine provided hierarchical interfaces between the FGS, dopamine, BST, and polymer matrix in the nanocomposites, and an increased number of dipoles were

incorporated in the nanocomposites with the inclusion of multiphase fillers.[16, 18] (iii) The high permittivity of the ferroelectric ceramic BST contributes to the permittivity of the nanocomposite.[38]

In many cases the permittivity of percolative composites dramatically increases with increasing conductive filler content, especially when the filler loading is close to the percolation threshold. However, ideal dielectric materials should simultaneously exhibit a high permittivity and low dielectric loss, which is not often achieved in such systems.[10-12] In our work (Figure 4b), the dielectric loss of the percolative composites shows the similar feature to the ceramic/polymer composites, which do not exhibit a large increase in loss with an increase of filler loading. For example, the dielectric loss remains low at a value of 0.084 at 1 kHz even when the FGS loading increased to 6.12 vol%, and the maximum dielectric loss of the nanocomposite with 7.19 vol% FGS was still relatively low ($\tan\delta$ =0.114); such properties are more attractive than most of the ceramic/polymer or traditional conductive particles/polymer composites (see Table 1). The dielectric loss in percolative composites mainly originates from space charge conduction, thus the insulation of the conductive filler such as graphene nanosheets is the key to decrease the dielectric loss, the use of simple organic modification usually lead to high dielectric loss due to most of the surface of graphene being bare, which is attributed to the difficulty in distributing reaction groups across the large specific surface area of graphene.[28] The nanocomposite with Dop@BST@FGS exhibited excellent insulation due to the low dielectric loss and electrical conductivity (Figure 4b and 4c). Charge carriers in the interfaces are not

free due to the FGS being prevented from connecting and forming conduction paths by the BST nanocuboid insulator embedded in the surface of the FGS. This composite architecture also led to an even distribution of the FGS in the polymer matrix, thus the accumulated charge carriers were trapped at the interfaces without a conductive channel path. In addition, an outer modification layer of dopamine makes the filler tightly adhere with the matrix so that voids or crack defects were mostly restricted.

Figure 4d shows the permittivity and dielectric loss of P(VDF-HFP) nanocomposites with Dop@BST@FGS, BST@FGS, fRGO,[1] and FGS as a function of mass fraction of FGS at 1 kHz (Supporting Information Figure S9). It can be seen that the permittivity of the Dop@BST@FGS/P(VDF-HFP) nanocomposites continuously increase with the Dop@BST@FGS content, while the nanocomposites with BST@FGS, fRGO and FGS all showed a low percolation threshold due to the high dielectric loss. It is clear that sample with Dop@BST@FGS exhibited a low dielectric loss, while the dielectric loss of the nanocomposites with the fillers such as fRGO and FGS exhibited an increase in loss with low filler loadings (see Figure 4d). The strong adhesion between the fillers and polymer matrix played an important role to the dielectric properties of the nanocomposites as Dop@BST@FGS and BST@FGS were introduced to the polymer matrix, the cross sectional SEM images of the sample films were shown (Supporting Information Figure S10). Due to the phase separation between BST@FGS and matrix, the BST@FGS/P(VDF-HFP) showed suppressed permittivity, significantly increased dielectric loss and electric conductivity compared to the uniform films with tightly adhered Dop@BST@FGS

fillers.

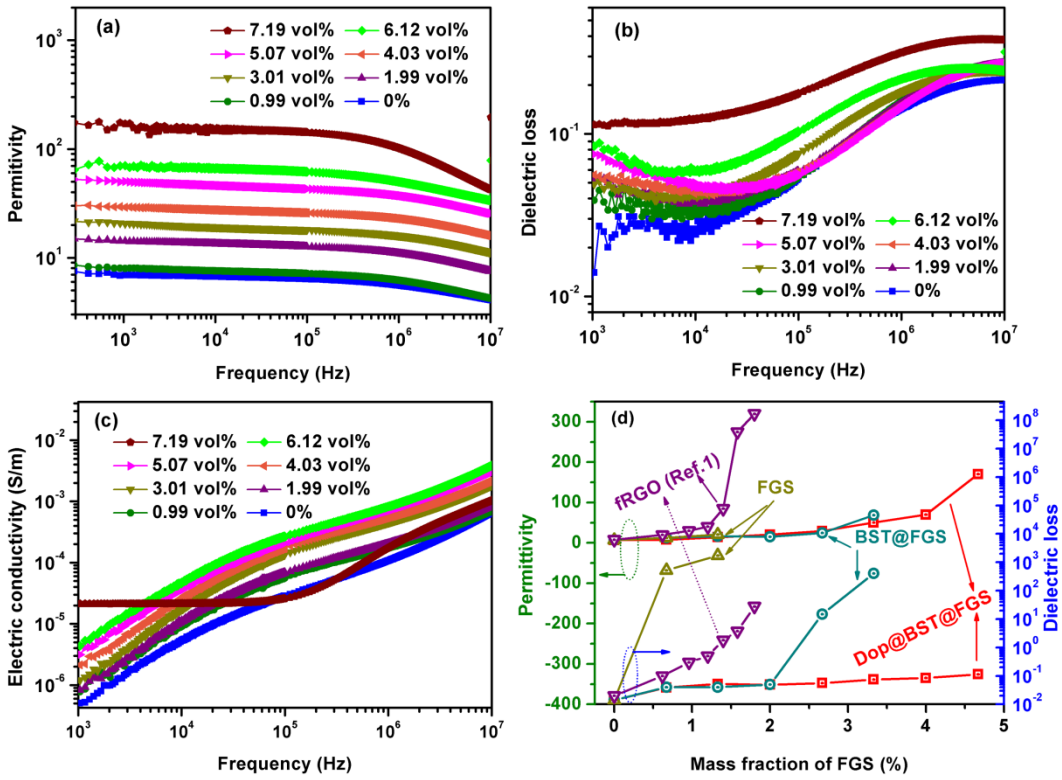

Figure 4. (a) Permittivity, (b) dielectric loss, (c) ac conductivity of Dop@BST@FGS/P(VDF-HFP) nanocomposites as a function of frequency with the volume fraction of FGS. (d) Permittivity and dielectric loss of P(VDF-HFP) nanocomposites with Dop@BST@FGS, BST@FGS, fRGO (Ref. 1) and FGS as a function of mass fraction of FGS at 1 kHz.

Percolation threshold (f_c) is a key parameter of percolative nanocomposite systems. The electrical conductivity and dielectric permittivity of the composites would increase by several orders of magnitude near the f_c, which can be used to evaluate the effective FGS loading by the following percolation theory equation (1):[10]

$$\varepsilon = \varepsilon_{matrix} \left| \frac{f_c - f_{FGS}}{f_c} \right|^{-s} \quad (1)$$

where ε_{matrix} is the permittivity of the P(VDF-HFP) matrix (6.9 at 1 kHz), ε is the permittivity of the nanocomposites at 1kHz, f_{FGS} is the volume fraction of the FGS, and s is a critical exponent.[39] The f_c of Dop@BST@FGS/P(VDF-HFP) and BST@FGS/P(VDF-HFP) nanocomposites respectively are 0.104 and 0.058 from the nonlinear fitting results shown in Figure S8a and b.

Breakdown strength is another important parameter of dielectric composite. Table 2 summarized the dielectric properties at 1 kHz and breakdown strength at 100 Hz of Dop@BST@FGS/P(VDF-HFP) nanocomposites with increased volume fraction of FGS. As can be seen that the nanocomposites keep a high level of breakdown strength when the FGS loading is less than 4.03 vol%, while the breakdown strength of the nanocomposite with 5.07 vol% is suddenly decreased to 53.8 MV/m, and the breakdown strength continuously decreased to 13.8 MV/m with the FGS loading increased to 7.19%. The f_c is determined by 0.104, which is not consistent with the catastrophe point of 5.07 vol%. Due to the BST nanocuboid prevent the FGS from aggregating and dopamine modified the surfaces of the fillers, the Dop@BST@FGS/P(VDF-HFP) nanocomposites with low FGS loadings show excellent insulativity and high breakdown strength. However, BST nanocuboid in nanocomposites possesses great difference of dielectric properties with the FGS and matrix, which lead to the local field concentration in the nanocomposite, thus the breakdown strength is suddenly decreased when the FGS loadings increased.

Table 2 Dielectric properties and breakdown strength of Dop@BST@FGS/P(VDF-HFP) nanocomposites with FGS loading.

Content of FGS(vol%)	0	0.99	1.99	3.01	4.03	5.07	6.12	7.19
Permittivity	6.9	7.9	14.2	20.5	29.1	50.2	70.2	170.4
Dielectric loss	0.014	0.039	0.052	0.049	0.056	0.075	0.084	0.114
Electric conductivity ($\times 10^{-6}$ S/m)	0.50	0.78	0.82	1.20	2.10	3.10	4.40	21.0
Breakdown strength (MV/m)	398	290	245	225	215	53.8	19.2	13.8

The permittivity, dielectric loss and electric conductivity are measured at 1 kHz, the breakdown strength is measured at 100 Hz.

CONCLUSIONS

In summary, a novel dielectric Dop@BST@FGS/P(VDF-HFP) nanocomposite with hierarchical interfaces was prepared and characterized in detail. The optimized percolative composite combined the high permittivity from a percolative composite with the low dielectric loss from an insulative composite. A high permittivity of 170.4 and low dielectric loss of 0.114 were achieved. This research broadens the range of traditional insulative and percolative composites, and provides a potential practical application in high performance dielectric composites.

Supporting Information

Supporting Information is available from the Online Library or from the author.

ACKNOWLEDGMENTS

This work was financially supported by Graduate Student Research Innovation Project in Hunan Province (no. 150140011), the National Natural Science Foundation of China (no. 51172288), and supported by State Key Laboratory of Powder Metallurgy, Central South University, Changsha, China.

REFERENCES

1. Wang, D.; Zhou, T.; Zha, J.-W.; Zhao, J.; Shi, C.-Y.; Dang, Z.-M, *J. Mater. Chem. A* **2013**, 1, 6162.

2. K. Yang, X. Y. Huang, J. L. He , and P . K. Jiang, *Adv. Mater. Interfaces* **2015**, *2*, 1500361.

3. S. Cho , J. S. Lee, J. Jang, *Adv. Mater. Interfaces **2015**, 2, 1500098*.

4. G. Wang, X. Y. Huang, P. K. Jiang, *ACS Appl. Mater. Interfaces* **2015**, 7, 18017.

5. D. Wang, Y. Bao, J. W. Zha, J. Zhao, Z. M Dang, G. H. Hu, *ACS Appl. Mater. Interfaces* **2012**, 4, 6273.

6. H. Luo, D. Zhang, L. Wang, C. Chen, J. Zhou and K. C. Zhou, *RSC Adv*. **2015**, 5, 52809.

7. H. Luo, Z. Wu, C. Chen, K. C. Zhou, and D. Zhang, *Composites Part A*, **2016**, 86, 57.

8. H. Luo, D. Zhang, C. Jiang, X. Yuan, C. Chen, K. Zhou, ACS Appl. Mater. Interfaces **2015**, 7, 8061.

9. H. Luo, C. Chen, K. C. Zhou, X. F. Zhou, Z. Wu, D. Zhang, *RSC Adv.* **2015**, 5, 68515.

10. K. Yang, X. Huang, L. Fang, J. He, P. Jiang, Nanoscale **2014**, 6, 14740.

11. Z. M. Dang, L. Wang, Y. Yin, Q. Zhang, Q. Q. Lei, Adv. Mater. **2007**, 19, 852.

12. C. Wu, X. Huang, L. Xie, X. Wu, J. Yu, P. Jiang, J. Mater. Chem. **2011**, 21, 17729.

13. C. Andrews, Y. Lin, H. A. Sodano, *Smart Mater. Struct.* **2010**, 19, 025018.

14. C. Wu, X. Huang, X. Wu, L. Xie, K. Yang, P. Jiang, Nanoscale **2013**, 5, 3847.

15. W. Li, F. Wang, Y. Liu, J. Wang, J. Yang, L. Zhang, A. A. Elzatahry, D. Al-Dahyan, Y. Xia, D. Zhao, *Nano Lett.* **2015**, 15, 2186.

16. J. Li, *Phys. Rev. Lett.* **2003**, 90, 217601.

17. Y. Chen, S. Zhang, X. Liu, Q. Pei, J. Qian, Q. Zhuang, Z. Han, Macromol. **2015**, 48, 365.

18. L. L. Sun, B. Li, Y. Zhao, G. Mitchell, W. H. Zhong, Nanotechnology **2010**, 21, 305702.

19. S. K. Patil, M. Koledintseva, R. W. Schwartz, W. Huebner, J. Appl. Phys. **2008**, 104, 074108.

20. H. Tang, G. J. Ehlert, Y. Lin, H. A. Sodano, Nano Lett. **2011**, 12, 84.

21. H. Pan, Y.-S. Hu, L. Chen, Energy Environ. Sci. **2013**, 6, 2338.

22. S. Cho, J. S. Lee, J. Jang, ACS Appl. Mater. Interfaces **2015**, 7, 9668.

23. J. W. Zha, T. X. Zhu, Y. H. Wu, S. J. Wang, R. K. Li, Z. M. Dang, J. Mater. Chem. C **2015**, 3, 7195.

24. Q. Guo, Q. Xue, J. Sun, M. Dong, F. Xia, Z. Zhang, Nanoscale **2015**, 7, 3660.

25. Y. Wang, J. Yu, W. Dai, D. Wang, Y. Song, H. Bai, X. Zhou, C. Li, C.-T. Lin, N. Jiang, RSC Adv. **2014**, 4, 59409.

26. A. C. Lopes, S. A. Carabineiro, M. F. R. Pereira, G. Botelho, S. Lanceros‐Mendez, ChemPhysChem **2013**, 14, 1926.

27. C. Min, D. Yu, J. Cao, G. Wang, L. Feng, Carbon **2013**, 55, 116.

28. M. Li, X. Huang, C. Wu, H. Xu, P. Jiang, T. Tanaka, J. Mater. Chem. **2012**, 22,

23477.

29. Y. Li, X. Huang, Z. Hu, P. Jiang, S. Li, T. Tanaka, ACS Appl. Mater. Interfaces **2011**, 3, 4396.

30. C. X. Guo, H. B. Yang, Z. M. Sheng, Z. S. Lu, Q. L. Song, C. M. Li, Angew. Chem. Int. Ed. **2010**, 49, 301.

31. Z. Liu, Q. Liu, Y. Huang, Y. Ma, S. Yin, X. Zhang, W. Sun, Y. Chen, Adv. Mater **2008**, 20, 3924.

32. R. Schafranek, S. Payan, M. Maglione, A. Klein, Physical Review B 2008, 77, 195310

33. S. Hirsch, P. Komissinskiy, S. Flege, S. Li, K. Rachut, A. Klein, L. Alff, J. Appl. Phys. **2014**, 115, 243704.

34. H. Xia, C. Hong, B. Li, B. Zhao, Z. Lin, M. Zheng, S. V. Savilov, S. M. Aldoshin, Adv. Funct. Mater. **2015**, 25, 627.

35. S. Yang, X. Song, P. Zhang, J. Sun, L. Gao, Small **2014**, 10, 2270.

36. A. Ferrari, J. Meyer, V. Scardaci, C. Casiraghi, M. Lazzeri, F. Mauri, S. Piscanec, D. Jiang, K. Novoselov, S. Roth, Phys. Rev. Lett. **2006**, 97, 187401.

37. G. Tian, J. Song, J. Liu, S. Qi, D. Wu, Soft Mater. **2014**, 12, 290.

38. M. Zhu, X. Huang, K. Yang, X. Zhai, J. Zhang, J. He, P. Jiang, ACS Appl. Mater. Interfaces **2014**, 6, 19644.

39. Z. M. Dang, J. P. Wu, H. P. Xu, S. H. Yao, M. J. Jiang, J. B. Bai, Appl. Phys. Lett.

2007, 91, 072912.

Table of Contents Graphic:

A noval percolative nanocomposite with super-high permittivity and surpressed dielectric loss is achieved, which is due to the hierarchical interfaces induced by $BaSrTiO_3$ nanocuboid dotted graphene sheets and further modification of dapamine.